Supporting Information:

Two-Dimensional Layers of Colloidal CdTe Quantum Dots: Assembly, Optical Properties and Vibroelectronic Coupling

Thomas Noblet,*†‡ Souhir Boujday,¶ Christophe Méthivier,¶ Marie Erard,† Julie Hottechamps,‡ Bertrand Busson† and Christophe Humbert†

† Université Paris-Saclay, CNRS, Institut de Chimie Physique, UMR 8000, 91405, Orsay, France.

‡ GRASP-Biophotonics, CESAM, University of Liege, Institute of Physics, Allée du 6 août 17, 4000 Liège, Belgium.

¶ Sorbonne Universités, UPMC Univ. Paris 6, UMR CNRS 7197 Laboratoire de Réactivité de Surface, F75005 Paris, France.

email: t.noblet@uliege.be

Number of pages: 7
Number of figures: 7

(I) Data extracted from XPS measurements

The XPS measurements performed on Si-APTES samples, as shown in the manuscript (Figure 2), enabled us to extract, first, the thicknesses of SiO_2 and APTES and, second, the density of APTES. To do so, we followed these steps:

1) Computation of the mean free paths $\xi^{M}_{X:nl}$ of the electrons associated to the states $|nl\rangle$ for each chemical element X in matrix M : we used the program *Quases*, based on S. Tanuma, C. J. Powell, D. R. Penn, *Surface and Interface Analysis* **21**, 165 (1994). The results are:

$$\xi^{APTES}_{Si:2p} = 3.6\ nm, \quad \xi^{SiO_2}_{Si:2p} = 3.7\ nm, \quad \xi^{Si}_{Si:2p} = 3.1\ nm \quad \text{and} \quad \xi^{APTES}_{C:1s} = 3.2\ nm.$$

2) Computation of the thickness of SiO_2 from the ratio between $I^{SiO_2}_{Si:2p}$, the intensity of the XPS peak associated to the state 2p of Si atoms within the oxyde layer, and $I^{Si}_{Si:2p}$, the intensity of the XPS peak associated to the state 2p of Si atoms within the substrate. From the Beer-Lambert law:

$$d_{SiO_2} = \xi^{SiO_2}_{Si:2p} \ln\left(1 + \underbrace{\frac{I^{SiO_2}_{Si:2p}}{I^{Si}_{Si:2p}}}_{0{,}25} \cdot \frac{\rho_{Si}\ \mathcal{M}_{SiO_2}\ \xi^{Si}_{Si:2p}}{\rho_{SiO_2}\ \mathcal{M}_{Si}\ \xi^{SiO_2}_{Si:2p}}\right) = 1\ nm,$$

where ρ and $\mathcal{M}$ denote the mass per unit volume and the molecular weight.

3) Computation of the thickness of APTES from the ratio between $I^{APTES}_{C:1s}$, the intensity of the XPS peak associated to the state 1s of C atoms within the layer of APTES, and $I^{Si}_{Si:2p}$. From the Beer-Lambert law:

$$\frac{I^{APTES}_{C:1s}}{I^{Si}_{Si:2p}} = \frac{9\ \dfrac{\rho_{APTES}}{\mathcal{M}_{APTES}}\ \sigma_{C:1s}\ \xi^{APTES}_{C:1s}\left(1 - \exp\left(-\dfrac{d_{APTES}}{\xi^{APTES}_{C:1s}}\right)\right)}{\dfrac{\rho_{Si}}{\mathcal{M}_{Si}}\ \sigma_{Si:2p}\ \xi^{Si}_{Si:2p}\ \exp\left(-\dfrac{d_{SiO_2}}{\xi^{SiO_2}_{Si:2p}}\right)\ \exp\left(-\dfrac{d_{APTES}}{\xi^{APTES}_{Si:2p}}\right)} = 0.28 \qquad \text{(eq. a)}$$

The photoionisation cross-sections were extracted from J. H. Scofield, *J. Electron Spectrosc. Relat. Phenom.* **8**,129-137 (1976). Especially, $\sigma_{C:1s} = 1.00$, $\sigma_{Si:2p} = 0.814$ and $\sigma_{N:1s} = 1.77$ (unit : 22 200 barns, 1 barn = 10^{-28} m^2). Then, we solved this implicit equation thanks to the graph drawn in Figure S1, which leads to the thickness $d_{APTES} = 0.9\ nm$.

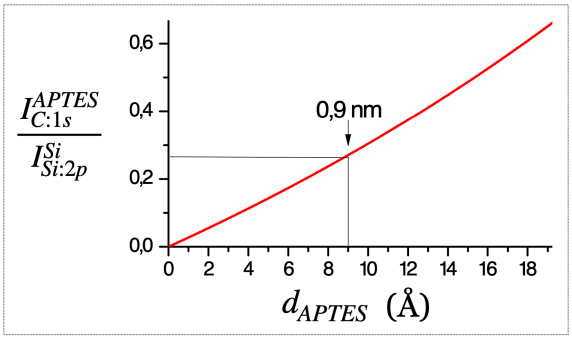

Figure S1 — Plot of the implicit equation (eq. a) to determine the thickness of APTES corresponding to the intensity ratio of 0.28.

4) Computation of the density of APTES from the ratio between $I_{N:1s}^{APTES}$, the intensity of the XPS peak associated to the state 1s of N atoms within the APTES layer, and $I_{Si:2p}^{Si}$. From the Beer-Lambert law:

$$N_{APTES} = \underbrace{\frac{I_{N:1s}^{APTES}}{I_{Si:2p}^{Si}}}_{0{,}041} \frac{\rho_{Si}}{\mathscr{M}_{Si}} \frac{\sigma_{Si:2p}}{\sigma_{N:1s}} \xi_{Si:2p}^{Si} \exp\left(-\frac{d_{SiO_2}}{\xi_{Si:2p}^{SiO_2}}\right) \exp\left(-\frac{d_{APTES}}{\xi_{Si:2p}^{APTES}}\right) = 1.7\ nm^{-2}.$$

(II) Data extracted from UV-visible measurements

We give additional UV-visible measurements in Figure S2, which support the results presented in Figure 4 (a). In order to fit the absorption spectra of Figures 4 (a) and S2, we used the following formula, adapted from [21]:

$$\mathscr{A}(\omega) = \frac{N_s}{2\,c\,\ln 10} \frac{\omega}{\hbar\varepsilon_0} \frac{1}{\sigma(R)}\sqrt{\frac{\pi}{2\epsilon_r}} \sum_{\nu=1}^{6} \frac{|p_\nu|^2}{G_\nu(\omega)} \exp\left(-\frac{(R_\nu(\omega)-R_0)^2}{2\,\sigma(R)^2}\right),$$

with:

$$R_\nu(\omega) = \frac{-\eta_\nu + \sqrt{\eta_\nu^2 + 4(\hbar\omega - E_g)\kappa_\nu}}{2(\hbar\omega - E_g)}, \text{ and } G_\nu(\omega) = \frac{2\kappa_\nu}{\hbar R_\nu^3(\omega)} - \frac{\eta_\nu}{\hbar R_\nu^2(\omega)}.$$

The two fitting parameters are N_s, the surface density of QDs, and $\sigma(R)$, the size dispersion. The other parameters are previously determined by applying the same formula to the absorption of a colloidal solution of QDs (whose concentration is known), with the difference that N_s must be substituted by the product $N \cdot \ell$ between the QD concentration N of the solution and the length ℓ of the cuvette. Here:

E_g	1,86 (eV)	p_5	9,4 (D)	η_6	0,21 (eV.nm)
ϵ_r	10,3	p_6	15,1 (D)	κ_1	2,39 (eV.nm²)
R_0	1,7 (nm)	η_1	0,25 (eV.nm)	κ_2	2,84 (eV.nm²)
p_1	10,7 (D)	η_2	0,21 (eV.nm)	κ_3	2,96 (eV.nm²)
p_2	4,4 (D)	η_3	0,25 (eV.nm)	κ_4	3,05 (eV.nm²)
p_3	1,2 (D)	η_4	0,25 (eV.nm)	κ_5	3,80 (eV.nm²)
p_4	4,9 (D)	η_5	0,21 (eV.nm)	κ_6	4,89 (eV.nm²)

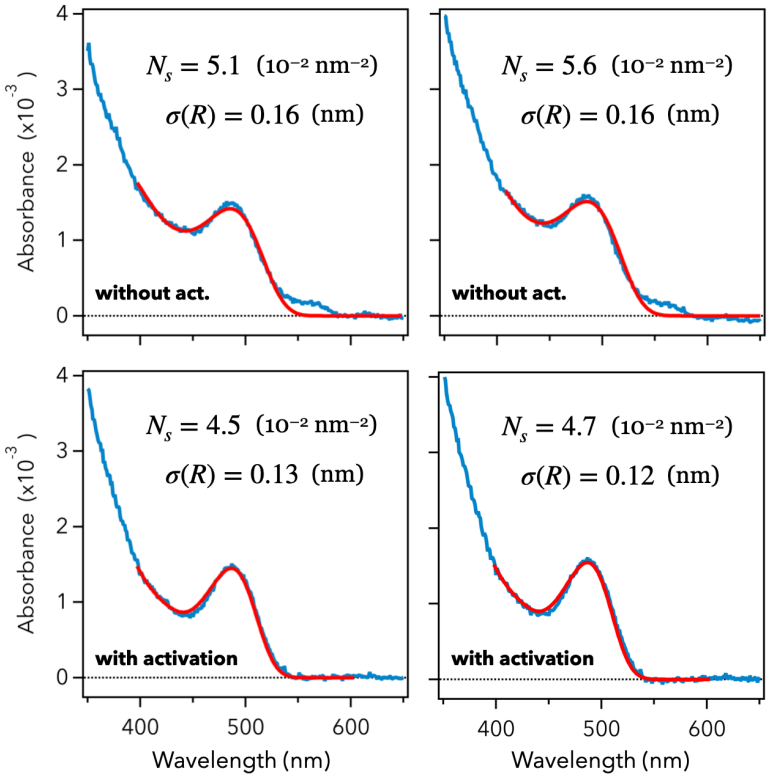

Figure S2 — Additional UV-visible spectra of Glass-APTES-QD(*) samples obtained with or without activation. This supports the results shown in Figure 4 (a).

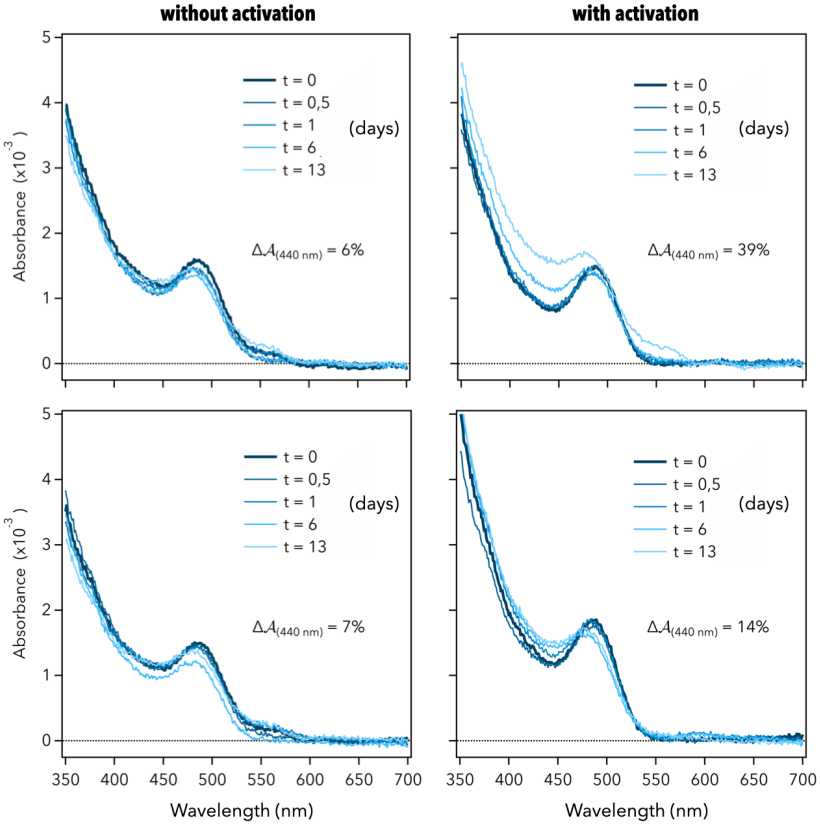

Figure S3 — Additional kinetic study of UV-visible spectra of Glass-APTES-QD(*) samples obtained with or without activation. This supports the results shown in Figure 4 (b).

In the manuscript, Figure 4 (b), we compute the standard deviation $\Delta\mathscr{A}_{440nm}$ of the UV-vis absorption to quantify the time stability of Glass-APTES-QD(*) samples. It is given by:

$$\Delta\mathscr{A}_{(440\text{ nm})} = \sqrt{\frac{1}{5}\sum_{t=0}^{13\text{ days}} \left(\mathscr{A}_{(440\text{ nm})}(t) - \langle\mathscr{A}_{(440\text{ nm})}\rangle\right)^2},$$

and express in percentage of the initial value $\Delta\mathscr{A}_{440nm}(t=0)$. We give additional measurements in Figure S3, which support the results presented in Figure 4 (b).

(III) Fluorescence decays of colloidal QDs and QD monolayers

The fluorescence decay of colloidal QDs (simply dispersed in water) constitutes the reference decay for which the QDs can be considered isolated (thanks to electrostatic repulsion). They are free to move and do not establish bonds with any species. To extract the corresponding fluorescence decay times τ_n, we used a triple exponential (Figure S4):

$$I_f(t) = \text{bkgnd} + \sum_{n=1}^{3} A_n\, e^{-t/\tau_n}.$$

For QD monolayers, it requires a sum of four exponentials (Figure S5).

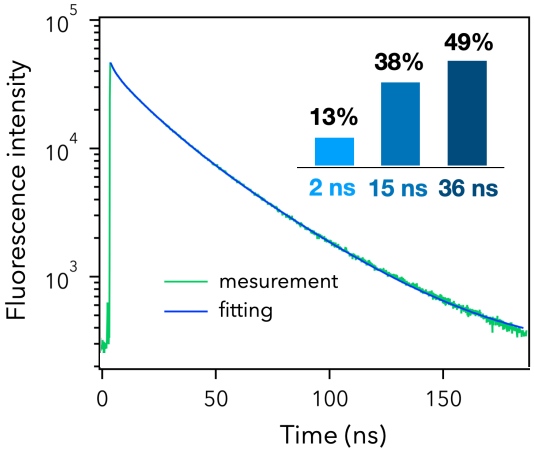

Figure S4 — Exponential modeling of the fluorescence decay of colloidal QDs with a tri-exponential fit function. The proportions of each lifetime are given by the histogram.

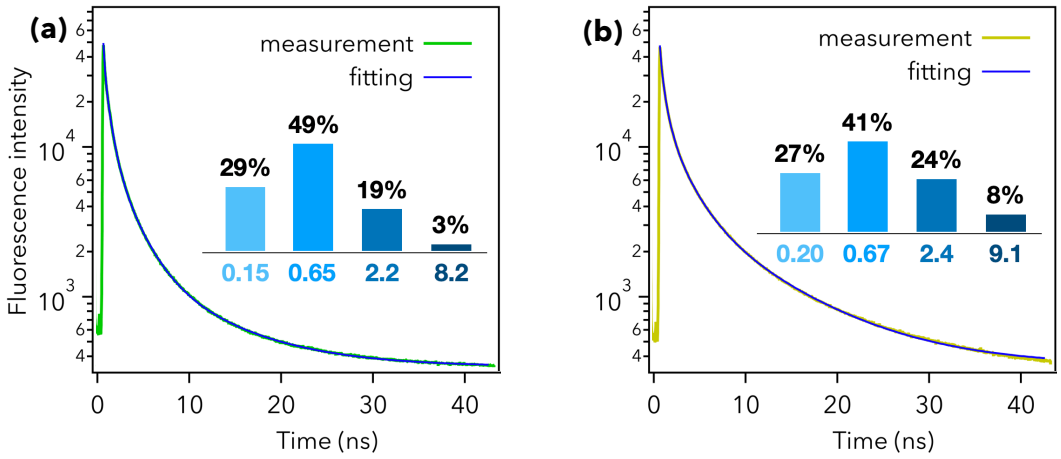

Figure S5 — Exponential modeling of the fluorescence decays of, **a**, physisorbed QDs and, **b**, chemisorbed QDs, with a quadri-exponential fit function. The proportions of each lifetime are given by the histogram.

(IV) Fluorescence decay of QD solids

In order to prove that the decreasing of the fluorescence lifetime observed for Glass-APTES-QD and Glass-APTES-QD* samples is due to a coupling between QDs and APTES and not to energy transfers between neighboring QDs (as it occurs within QD solids), we characterized a QD thick film with the same CdTe QDs. This film is obtained by the deposition of a colloidal droplet of 50 µL (0.5 µM) on a glass slide, dried by nitrogen. Figure S6 shows its emission spectrum and its time-resolved fluorescence profile. The fluorescence band undergo a strong redshift of 15 nm while the fluorescence lifetime drops to 2.4 ns. As demonstrated in Ref. [35] (*ChemPhysChem* **21**, 853-862, 2020), this spectral redshift is indeed due to QD-QD energy transfer.

In comparison, the QD monolayers characterized in the manuscript exhibit lifetimes of 1.0 and 1.6 ns, which suggests a stronger coupling than that of the QD solid above mentioned. But Figure 3 evidences a redshift of only 6 nm. If it was due to energy transfer between neighboring QDs, we would expect a spectral redshift of more than 15 nm. As a result, the observed decrease of the fluorescence lifetimes in the case of QD monolayers is well and truly related to the coupling between QDs and APTES.

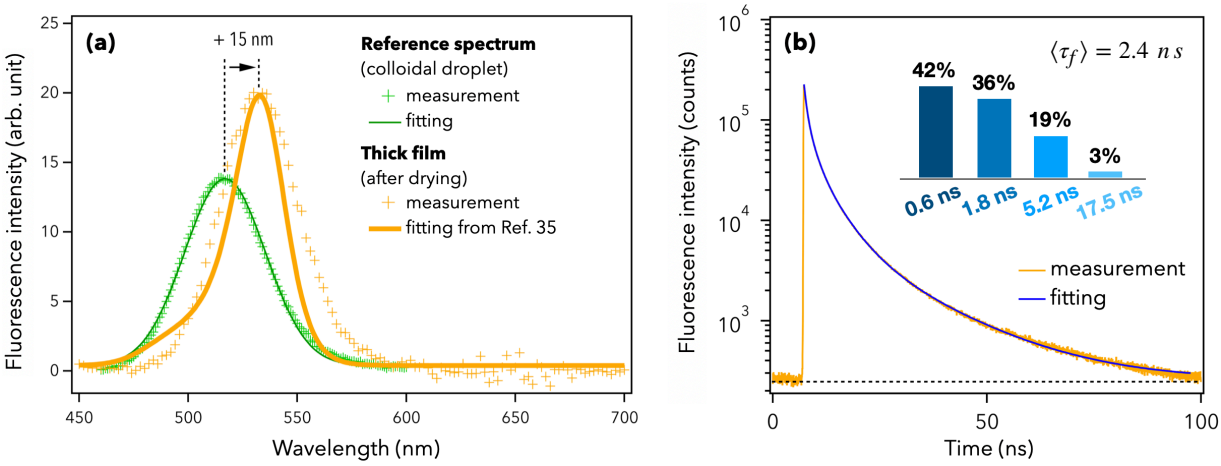

Figure S6 — a, UV-visible spectrum of a QD solid (thick film). **b**, Time-resolved fluorescence profile of the same QD solid.

(V) Fitting procedure of the SFG measurements

In order to fit the SFG spectra of Figure 6 (a, b), we used the common procedure given in Ref. [20]. The SFG intensity is modeled by:

$$I(\omega_{SFG}) \propto \frac{\omega_{SFG}^2}{\cos^2\theta_{SFG}} \left|\chi_{eff}^{(2)}(\omega_{vis},\omega_{IR})\right|^2 I(\omega_{vis})\, I(\omega_{IR}),$$

with:

$$\chi_{eff}^{(2)}(\omega_{vis},\omega_{IR}) = A\ e^{\imath\Phi} + \sum_v \frac{a_v\ e^{\imath\varphi_v}}{\omega_{IR}-\omega_v+\imath\gamma_v}.$$

This effective second-order nonlinear susceptibility is made of a non-resonant contribution $Ae^{\imath\Phi}$ assigned to the inorganic components of the sample, and an IR-resonant contribution assigned to the molecular vibrations. Each vibration mode $|v\rangle$ is then modeled by a lorentzian resonance centered at ω_v with the amplitude a_v and the width γ_v.

The following table gives the fitting parameters for Figure 6 (a, b). We considered only two vibration modes.

Glass-APTES (Fig. 4 b)			Glass-APTES-QD (Fig. 4 a)		
A	0.0076	($V^{1/2}$)	A	0.012	($V^{1/2}$)
Φ	4,7	(rad)	Φ	4,4	(rad)
a_1	0.055	($V^{1/2}$)	a_1	0.061	($V^{1/2}$)
φ_1	0	(rad)	φ_1	0	(rad)
ω_1	2937	(cm^{-1})	ω_1	2937	(cm^{-1})
γ_1	7.5	(cm^{-1})	γ_1	7.5	(cm^{-1})
a_2	0.072	($V^{1/2}$)	a_2	0.058	($V^{1/2}$)
φ_2	0	(rad)	φ_2	0	(rad)
ω_2	2962	(cm^{-1})	ω_2	2962	(cm^{-1})
γ_2	8.5	(cm^{-1})	γ_2	8.5	(cm^{-1})

(VI) Power-Wavelength dependence of the tunable visible and IR OPO

For SFG spectroscopy, we use two optical parametric oscillators (OPO) to generate the two tunable laser beams, over the visible and the IR ranges. Here we give their respective powers (at the sample point) over the probed spectral ranges (Figure S7).

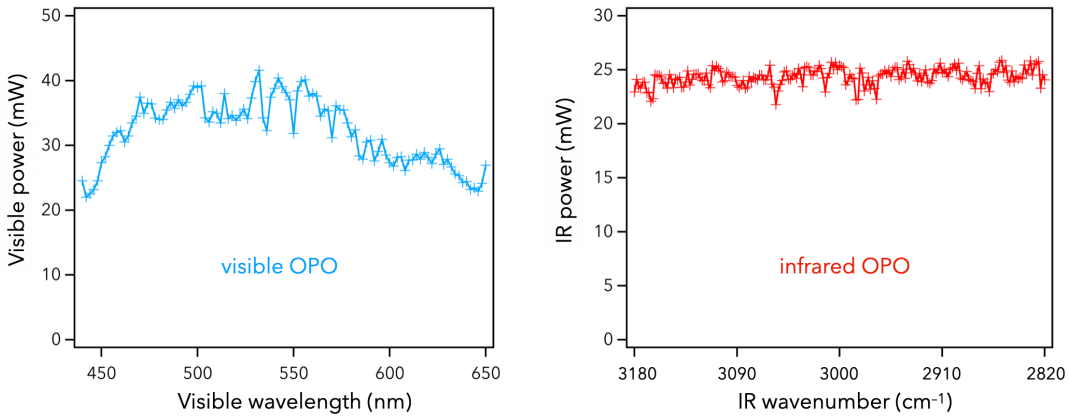

Figure S7 — Dependence of the visible and IR powers supplied by the two OPOs according to the visible wavelength and the IR wavenumber, respectively.